White Rose Research Online

eprints@whiterose.ac.uk
https://eprints.whiterose.ac.uk
Universities of Leeds, Sheffield and York

Deposited via The University of Sheffield.

White Rose Research Online URL for this paper:
https://eprints.whiterose.ac.uk/id/eprint/220100/

Version: Published Version

Article:
In Yoon, S., Park, H., Lee, Y. et al. (2024) Pressure enabled organic reactions via confinement between layers of 2D materials. Science Advances, 10 (45). eadp9804. ISSN: 2375-2548

https://doi.org/10.1126/sciadv.adp9804

Reuse
This article is distributed under the terms of the Creative Commons Attribution-NonCommercial (CC BY-NC) licence. This licence allows you to remix, tweak, and build upon this work non-commercially, and any new works must also acknowledge the authors and be non-commercial. You don't have to license any derivative works on the same terms. More information and the full terms of the licence here:
https://creativecommons.org/licenses/

Takedown
If you consider content in White Rose Research Online to be in breach of UK law, please notify us by emailing eprints@whiterose.ac.uk including the URL of the record and the reason for the withdrawal request.

UNIVERSITY OF LEEDS
University of Sheffield
UNIVERSITY of York

ORGANIC CHEMISTRY

Pressure enabled organic reactions via confinement between layers of 2D materials

Seong In Yoon[1]†, Hyoju Park[2,3]†, Yeonju Lee[4]†, Changding Guo[5,6], Yu Jin Kim[6], Joo Song Lee[6], Seungwoo Son[2,3], Myeonggi Choe[2,3], Daeho Han[4,7], Kidal Kwon[4], Jongyeong Lee[2,3], Kyung Yeol Ma[1], Amirreza Ghassami[4,8], Sung Wook Moon[4], Sun-Young Park[2,3,9], Bong Kyun Kang[10], Yoon-Jeong Kim[11,12], Seonghyun Koo[13], Armando Genco[14], Jaewoo Shim[15], Alexander Tartakovskii[14], Yunrui Duan[2,3], Feng Ding[2,3], Seokhoon Ahn[11], Sunmin Ryu[13], Ju-Young Kim[2,3], Woo Seok Yang[16], Manish Chhowalla[17]*, Young S. Park[4]*, Seung Kyu Min[3,4]*, Zonghoon Lee[2,3]*, Hyeon Suk Shin[1,3,4,5,6]*

Copyright © 2024 The Authors, some rights reserved; exclusive licensee American Association for the Advancement of Science. No claim to original U.S. Government Works. Distributed under a Creative Commons Attribution NonCommercial License 4.0 (CC BY-NC).

Confinement of reactants within nanoscale spaces of low-dimensional materials has been shown to provide reorientation of strained reactants or stabilization of unstable reactants for synthesis of molecules and tuning of chemical reactivity. While few studies have reported chemistry within zero-dimensional pores and one-dimensional nanotubes, organic reactions in confined spaces between two-dimensional materials have yet to be explored. Here, we demonstrate that reactants confined between atomically thin sheets of graphene or hexagonal boron nitride experience pressures as high as 7 gigapascal, which allows the propagation of solvent-free organic reactions that ordinarily do not occur under standard conditions. Specifically, we show that cyclodehydrogenation of hexaphenylbenzene without catalysts as a proof of concept and oxidative polymerization of dopamine into sheet-like crystalline structure are enabled by the effective high pressure experienced by the reactants between the graphene layers. Our results demonstrate a facile, general approach for performing high-pressure chemistry based on confinement of reactants within two-dimensional materials.

INTRODUCTION

Chemical reactions conducted at high pressures provide opportunities for realizing synthesis chemistries and achieving unique states of matter (*1*, *2*). Many industrial chemical reactors operate at pressures of few thousand atmospheres, but facile application of very high pressures (>1 GPa), where interesting reactions can occur and imaginary materials can be realized, is challenging. On the other hand, high pressure induced on molecules in solution, a liquid pocket, between two layers of graphene has been used to induce phase transitions of water (*3*), inorganic salts (*4*–*6*), and C_{60} (*7*). Such hermetically sealed liquid cells created have been also used for in situ observation of reaction dynamics of metal nanoparticles in transmission electron microscopy (TEM) (*8*–*11*).

It is well known that nanoconfinement can enhance chemical reactivity of reagents by increasing the local concentration, preorganizing the reagents for a conformation with favorable reactivity, and/or stabilizing the transition state (*12*, *13*). As an example of nanoconfinement, the mica hypothesis was proposed for providing several ideas on the origin of life on mineral surfaces, where mechanical energy is a major energy source for polymerization and confinement between mineral sheets induces entropy reduction for chiral biopolymer (*14*). While studies have been carried out using zero-dimensional (0D) and 1D confined spaces found in pores of zeolites or cages and carbon nanotubes (*15*–*21*), well-defined confined van der Waals (vdW) gap spaces between 2D materials (2DMs) offer simplicity, scalability, and well-controlled pressure due to upward and downward forces only (*22*, *23*).

Cyclodehydrogenation is widely used in organic reactions as a common strategy for the synthesis of polycyclic aromatic hydrocarbons (PAHs) including graphene nanoribbons (*24*–*27*). However, bottom-up synthesis of graphene nanoribbons has been achieved by surface-assisted, catalytic reactions through two-step thermal activation: (i) formation of linear polymer by dehalogenation and radical addition during deposition of specially designed monomers on metal substrate maintained at 200°C and (ii) subsequent cyclodehydrogenation of the linear polymer at 400°C (*24*–*27*). Hexabenzocoronene (HBC), a well-known PAH, is easily synthesized by the intramolecular oxidative cyclodehydrogenation of hexaphenylbenzene (HPB) with the aid of an acid catalyst and $FeCl_3$ oxidant in bulk solution (*28*, *29*). In this study, we demonstrate the cyclodehydrogenation of

[1]Department of Energy Engineering, Ulsan National Institute of Science and Technology (UNIST), Ulsan 44919, Republic of Korea. [2]Department of Materials Science and Engineering, Ulsan National Institute of Science and Technology (UNIST), Ulsan 44919, Republic of Korea. [3]Center for Multidimensional Carbon Materials, Institute for Basic Science (IBS), Ulsan 44919, Republic of Korea. [4]Department of Chemistry, Ulsan National Institute of Science and Technology (UNIST), Ulsan 44919, Republic of Korea. [5]Department of Energy Science and Department of Chemistry, Sungkyunkwan University (SKKU), Suwon 16419, Republic of Korea. [6]Center for 2D Quantum Heterostructures, Institute of Basic Science (IBS), Sungkyunkwan University (SKKU), Suwon 16419, Republic of Korea. [7]Department of Chemistry, University of Buffalo, The State University of New York, Buffalo, NY 14260, USA. [8]MAX IV Laboratory, Lund University, PO Box 118, SE-22100 Lund, Sweden. [9]Materials Safety Technology Research Division, Korea Atomic Energy Research Institute (KAERI), Daejeon 34057, Republic of Korea. [10]Department of Electronic Materials, Devices, and Equipment Engineering, Soonchunhyang University, 22, Soonchunhyang-ro, Asan City, Chungnam, 31538 Republic of Korea. [11]Institute of Advanced Composite Materials, Korea Institute of Science and Technology (KIST), Jeonbuk 55324, Republic of Korea. [12]Department of Chemistry, Hanyang University, Seoul 04763, Republic of Korea. [13]Department of Chemistry, Pohang University of Science and Technology (POSTECH), Pohang, Gyeongbuk 37673, Republic of Korea. [14]Department of Physics and Astronomy, University of Sheffield, Sheffield S3 7RH, UK. [15]Device Research Center, Samsung Advanced Institute of Technology, Suwon 18448, Republic of Korea. [16]Nano Materials and Components Research Center, Korea Electronics Technology Institute (KETI), Seongnam 13509, Republic of Korea. [17]Department of Materials Science and Metallurgy, University of Cambridge, Cambridge CB3 0FS, UK.
*Corresponding author. Email: mc209@cam.ac.uk (M.C.); youngspark@unist.ac.kr (Y.S.P.); skmin@unist.ac.kr (S.K.M.); zhlee@unist.ac.kr (Z.L.); shin0902@skku.edu (H.S.S.)
†These authors contributed equally to this work.

Downloaded from https://www.science.org on November 25, 2024

HPB to obtain HBC in solid-state 2DM sandwich structures as confined 2DM vessels with high vdW pressure by strong coupling of 2DMs through annealing at 200°C (*30*, *31*) and without any catalyst and oxidant (Fig. 1A). The cyclodehydrogenation of HPB does not occur under these conditions in the absence of confined 2DM vessels (fig. S1). Furthermore, there is no catalytic cyclodehydrogenation of HPB on graphene (fig. S2) and on Au surface (figs. S3 and S4). While the surface confinement effect is known to restrict the free movement or structural flexibility of molecules on the substrate to facilitate chemical reactions (*32*–*34*), the possibility of the cyclodehydrogenation reaction of HPB on graphene due to the surface confinement is very low (fig. S2).

RESULTS

To fabricate graphene/HPB/graphene (G/HPB/G) pressure vessels, HPB was spin-coated on as-grown chemical vapor deposition (CVD) graphene followed by transfer of another graphene layer (see Materials and Methods for details of CVD graphene transfer and dimensions of graphene layers). Studies with hexagonal boron nitride (hBN) layers in place of graphene are described in Materials and Methods). Cyclodehydrogenation of HPB was performed by heating G/HPB/G at 200°C for 180 min. The reason why we annealed the sandwich samples at 200°C is because the annealing makes the graphene (or hBN) sandwich strongly coupled; thus, vdW pressure is applied in the graphene (or hBN) sandwich. It is well known that the annealing between 150° and 350°C is required for strongly coupled graphene bilayer (*30*, *31*). Just the transfer of the top layer graphene to HPB/G cannot induce the strong coupling for applying vdW pressure. We could observe the cyclodehydrogenation of HPB to HBC even at lower temperatures than 200°C because of strong coupling even at lower temperatures (Fig. 1, G and H, and figs. S5 to S7). However, while the reaction occurs in local area, where vdW pressure is applied, at lower temperature than 200°C and the yield of the reaction increases with temperature, the reaction occurs everywhere in the sample after annealing at 200°C. It is also noted that the cyclodehydrogenation reaction may also be possible even within the sandwich structure prepared using bilayer graphene (fig. S8).

The Raman spectra of bilayer graphene prepared by the transfer of graphene (G/G), G/HPB/G, and thermally treated G/HPB/G to obtain G/HBC/G are shown in Fig. 1B. G/G spectrum in Fig. 1B is similar to turbostratic stacked graphene with 2D and G peak intensity ratio (I_{2D}/I_G) of 2.84 (*35*, *36*). The I_{2D}/I_G (2.10) ratio of G/HPB/G was found to be slightly lower because of weak π-π interactions between graphene layers and the aromatic rings of HPB due to the imperfect parallel orientation of HPB molecules with graphene (*37*, *38*). The I_{2D}/I_G ratio is affected by the change in electronic structure of graphene by doping, stacking order, or formation of superlattice. In contrast, a large reduction in the I_{2D}/I_G ratio (0.42) is observed for G/HBC/G samples, which indicates that the formation of the polyaromatic rings by HBC affects the electronic structure of graphene. This induces the zone-folding effect through superlattice formation, resulting in a decreased I_{2D}/I_G ratio (Fig. 1B) (*39*, *40*).

The formation of HBC between the graphene layers was confirmed by time-of-flight secondary ion mass spectroscopy (TOF-SIMS). For the TOF-SIMS measurements, the as-formed HBC between the graphene layers was exposed by removing the top layer by the peel-off method [see Fig. 1C, Materials and Methods, and (*41*)]. The TOF-SIMS results from HPB ($[M]^+$) [mass/charge ratio (*m/z*) 534.23] shown in Fig. 1D show a strong signal at *m/z* 535.24 ($[M + H]^+$), which denotes protonated HPB. As expected, the peak for HBC with the exact mass of *m/z* 522.14 appears at *m/z* 522.24. The hBN sandwich structure showed the same results (fig. S9). It is noted that a control experiments with commercial HBC (ATK Chemical Company Ltd.) in the graphene sandwich structure showed the same results for Raman and TOF-SIMS spectra (fig. S10). Moreover, the insulating nature of hBN allows absorption and photoluminescence (PL) measurements (not possible with semimetallic graphene) of hBN/HPB/hBN and hBN/HBC/hBN that also support the formation of HBC in Fig. 1 (E and F). Absorbance between 375 and 400 nm (Fig. 1E) and a strong PL peak at 410 to 700 nm (Fig. 1F) after heating were observed, which are attributed to the increase in aromaticity due to the formation of HBC and its aggregation (*42*). The small PL peaks (420 to 500 nm) in hBN and hBN/HPB/hBN are due to nitrogen vacancies (*43*).

The conversion of HPB to HBC in the confined graphene vessel after annealing can be also identified by high-resolution TEM (HR-TEM) images. We acquired HRTEM images of HPB and HBC molecules after annealing G/HPB/G samples at 65°, 100°, 150°, and 200°C. The conversion of HPB to HBC after annealing at 65°C is rare, and thus HBC molecules are observed in a very local area. However, HBC molecules are more likely to be found after annealing at 100° and 150°C. Most of isolated molecules are HBC after annealing at 200°C. Representatively, an isolated HPB molecule in the graphene sandwich after annealing at 150°C is shown in time-elapsed images of Fig. 1G, while Fig. 1H shows an isolated HBC molecule in the same sample. In addition, we are able to observe similar HPB and HBC molecules' configurations in the graphene vessel after annealing at 100°C (fig. S6). While atomic structures of HPB and HBC molecules are similar, their HRTEM images are very different from each other. In Fig. 1H, an HBC molecule shows rounded shape with brighter contrast at the edge due to the tighter bonding of carbon-carbon atoms in HBC with the loss of hydrogen atoms at the edge in the HRTEM image. However, an HPB molecule shows structural distortion in Fig. 1G because the six outer phenyl rings rotate very quickly under e-beam exposure for TEM measurement (higher degree of freedom in moving). It is noted that an HBC molecule is static under e-beam irradiation because outer phenyl rings do not rotate any more by C—C couplings. We summarize HRTEM images of HBC at different temperatures, 65°, 100°, 150°, and 200°C, in fig. S7. It is noted that we cannot assign carbons of the HPB molecule because of its distorted structure, but we can see the atomic structure of HBC in the confined graphene vessel by a careful measurement because HBC is relatively stable (fig. S11)—note that both HPB and HBC molecules move freely between graphene layers under e-beam irradiation (movies S1 and S2). The temperature-dependent HRTEM results are consistent with the temperature-dependent Raman results in fig. S5.

To further analyze how the confinement of reactants between layers of graphene by vdW pressure leads to the cyclodehydrogenation of HPB, we calculated the reaction energy profiles for the cyclodehydrogenation of HPB in the graphene sandwich based on density functional theory (see Materials and Methods). Figure 2 presents the reaction energy profile of the first dehydrogenation reaction with the corresponding structures, i.e., the reactant (HPB), the transition state, and the dehydrogenated product (HPB-2H). Relative energies with reference to the optimized HPB and the dihedral angles (ϕ) between the central benzene ring and outer phenyl rings for

Downloaded from https://www.science.org on November 25, 2024

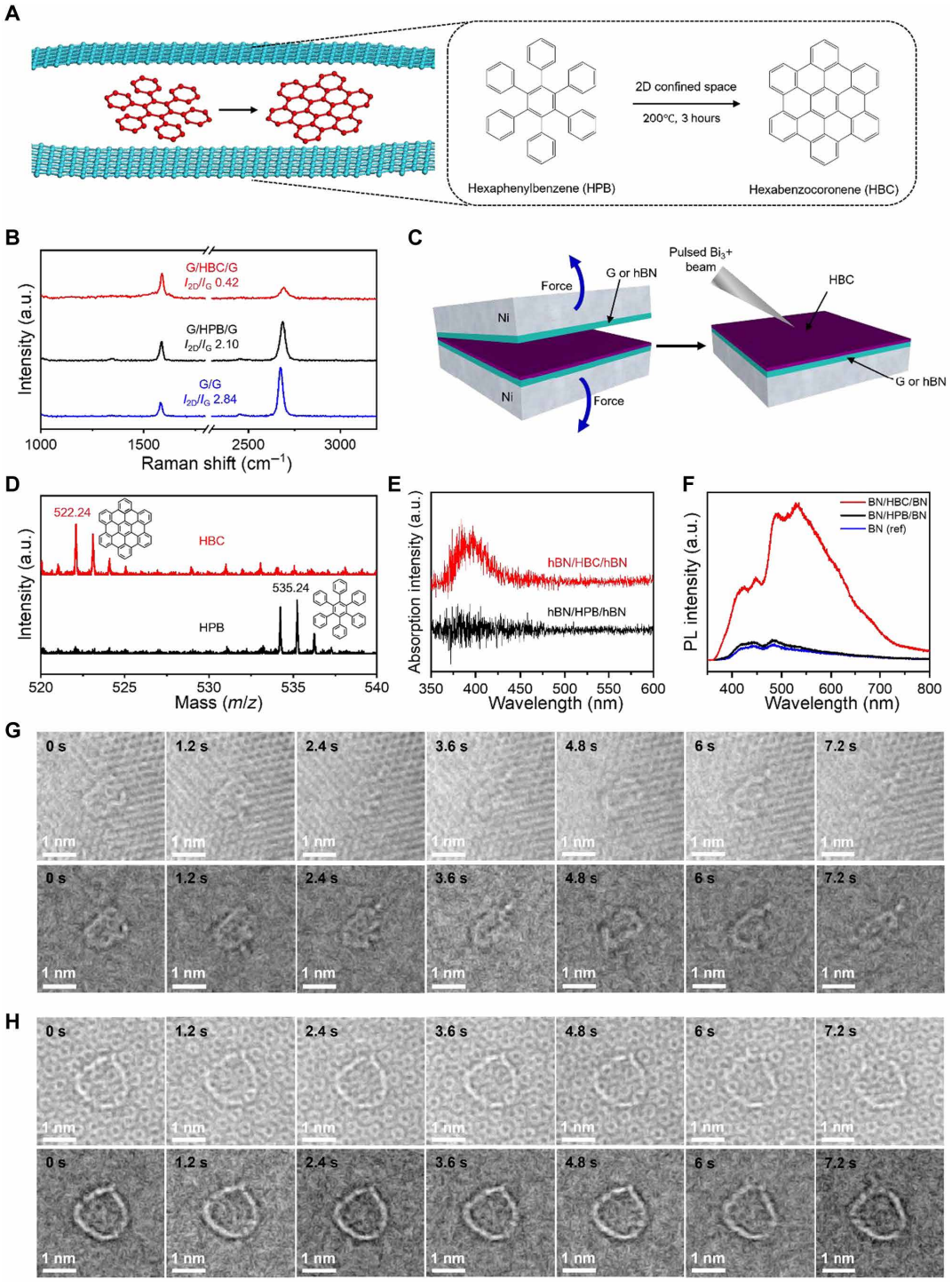

Fig. 1. Cyclodehydrogenation reaction of HPB between layers of graphene or hBN. (**A**) Schematic illustration of cyclodehydrogenation of HPB confined between graphene layers. (**B**) Raman spectra of G/G, G/HPB/G, and G/HBC/G. (**C**) Schematic illustration of peeling of graphene layers by Ni deposition on both sides of the vessel. (**D**) TOF-SIMS results of HPB and HBC between graphene layers before and after heat treatment at 200°C, respectively. The data acquisition time was 20 s. (**E**) Absorption spectra (derived from reflectance measurement) of hBN/HPB/hBN before and after heat treatment. (**F**) Comparison of photoluminescence (PL) spectra of BN/HPB/BN before and after heat treatment. Excitation wavelength is 340 nm. (**G** and **H**) High-resolution TEM (HRTEM) images of HPB and HBC in a confined graphene vessel after annealing G/HPB/G at 150°C for 180 min. (G) Sequential images of HPB confined in the graphene sandwich (top) and corresponding sequential IFFT images (bottom) after removing top and bottom graphene lattices. (H) Sequential images of HBC confined in the graphene sandwich (top) and corresponding sequential inverse fast Fourier transform (IFFT) images (bottom) after removing top and bottom graphene lattices. To obtain a clear contrast for HPB and HBC molecules, corresponding IFFT images were acquired after eliminating the reflection spots from graphene lattices. HRTEM images were obtained in fast sequential imaging (an exposure time of 0.1 s and an interval time of 1.1 s). a.u., arbitrary units.

Downloaded from https://www.science.org on November 25, 2024

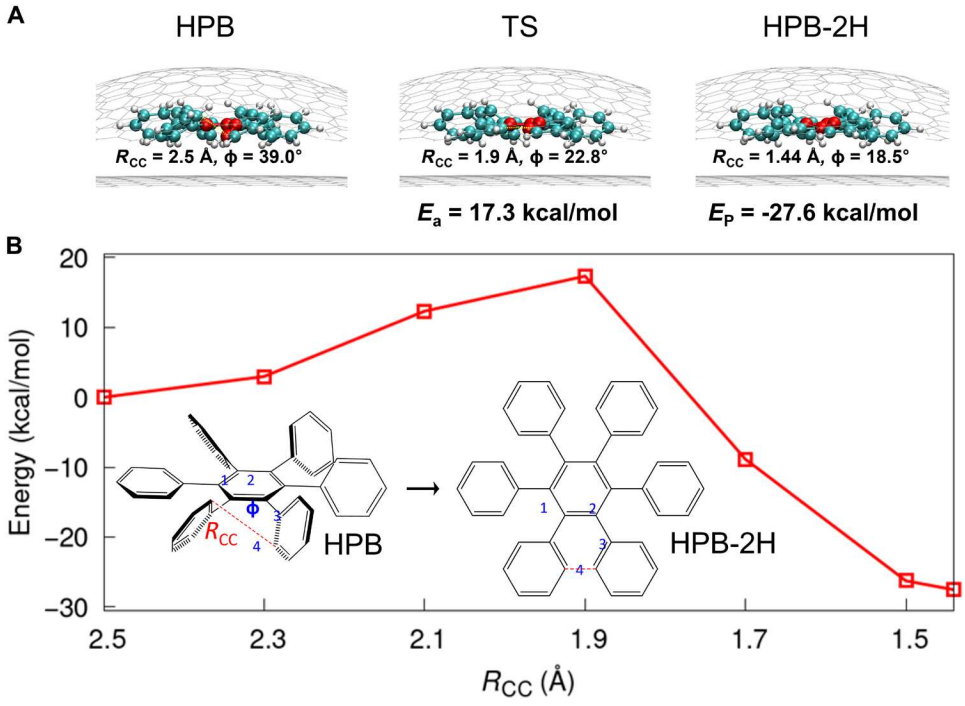

Fig. 2. Reaction energy profile and corresponding optimized structures for the first cyclodehydrogenation reaction of HPB confined in graphene layers based on the density functional theory calculations. (**A**) Structures of HPB, the transition state (TS), and the product (HPB-2H) from the first cyclodehydrogenation of HPB confined in graphene layers. Distances between two carbons for the bond formation (RCC) and dihedral angles (ϕ) between the central benzene and the outer phenyl ring are specified. (**B**) Energy profile in kilocalories per mole (kcal/mol) with respect to the bond formation of two carbon atoms. The inset figure represents the first dehydrogenation reaction where we represent the distance between carbon atoms as RCC and the dihedral angle (ϕ) with four carbon atoms labeled as 1 to 4 (red atoms in the upper structures).

dehydrogenation are also displayed. Since the estimated reaction energy barrier is 17.3 kcal/mol, which is similar to the known barrier with strong oxidants at ambient temperature, ~16 kcal/mol, for the arenium cation pathway (*29*), we expect that the dehydrogenation under the vdW pressure is possible. It is noted that there was no geometry showing bonding between hydrogen atoms and carbon atoms in the graphene layers during the computation, suggesting that the graphene is inert during the dehydrogenation. On the basis of ab initio force analysis [see fig. S12 (A and B) for atomic force components], the estimated pressure applied to the sandwiched HPB is 6.83 and 7.3 GPa for graphene and hBN sandwiches, respectively, at the interlayer distance of 0.7 nm, which is higher than the estimated vdW pressure with large-sized graphene bubbles (*6*). The molecule-sized vessel with a height < 1 nm can achieve a vdW pressure > 1 GPa, and a value as high as 70 GPa has been reported for atomic clusters under a graphene sheet (*44*). Our calculation results show that high pressure within sandwiched graphene or hBN flattens HPB and lowers the energy barrier to enable its cyclodehydrogenation reaction at 200°C. We also calculated the large-scale sandwiched structures based on semi-empirical and empirical calculations with 31 HPB and 50 HPB molecules, respectively. In case of a cluster of 50 HPB molecules (the height with respect to the upper graphene layer (*h*) of 1.08 nm and the diameter (2*R*) of 12.3 nm), the estimated vdW pressure based on the force component analysis as G/HPB/G becomes 0.58 GPa while the pressure with 31 HPB molecules ($h = 0.84$ nm and $2R = 8.9$ nm) shows the vdW pressure of 3.16 GPa (fig. S12, C and D). From the statistical analysis, dihedral angles of approximately 12 to 29% HPB molecules in the large-scale sandwiched structures are smaller than ~39° for G/HPB/G, which makes the dehydrogenation reaction plausible for large-scale sandwiched structures. In addition, we theoretically studied the mechanism because it is difficult to take only the intermediate out from the sandwich structure to understand the mechanism. We investigated the reaction energy profile for the synchronous and stepwise cyclic dehydrogenation reactions based on the density functional theory calculations for the isolated HPB molecule. The energy barrier of the synchronous reaction was 1047.3 kcal/mol, while the energy barrier of the stepwise reaction was 190.4 kcal/mol (fig. S13), suggesting that the cyclodehydrogenation occurs through the stepwise reaction.

We now discuss the polymerization of dopamine as another example of pressure-induced reaction between graphene layers. Dopamine is generally oxidatively polymerized in basic solution (Fig. 3A). Bulk polydopamine is known to be an amorphous polymer with three linear, randomly distributed components (dopamine, 5,6-dihydroxyindole, and leukodopaminechrome) (fig. S14A) (*45*–*47*). Crystalline polytype of polydopamine has not been observed to date. We have found that polymerization of dopamine in the confined space between two graphene layers forms the unique polycrystalline oligomers of low molecular weight (Fig. 3A). In addition to the effect of pressure (flattened dopamine) in the graphene-confined space, we also find that graphene layers play a role in preventing reaction of dopamine monomers with environmental oxygen or water so that random oxidative polymerization is suppressed. It is known that the reduction of oxygen in the dopamine solution led to a decrease in the polymerization kinetics (*45*–*47*).

Downloaded from https://www.science.org on November 25, 2024

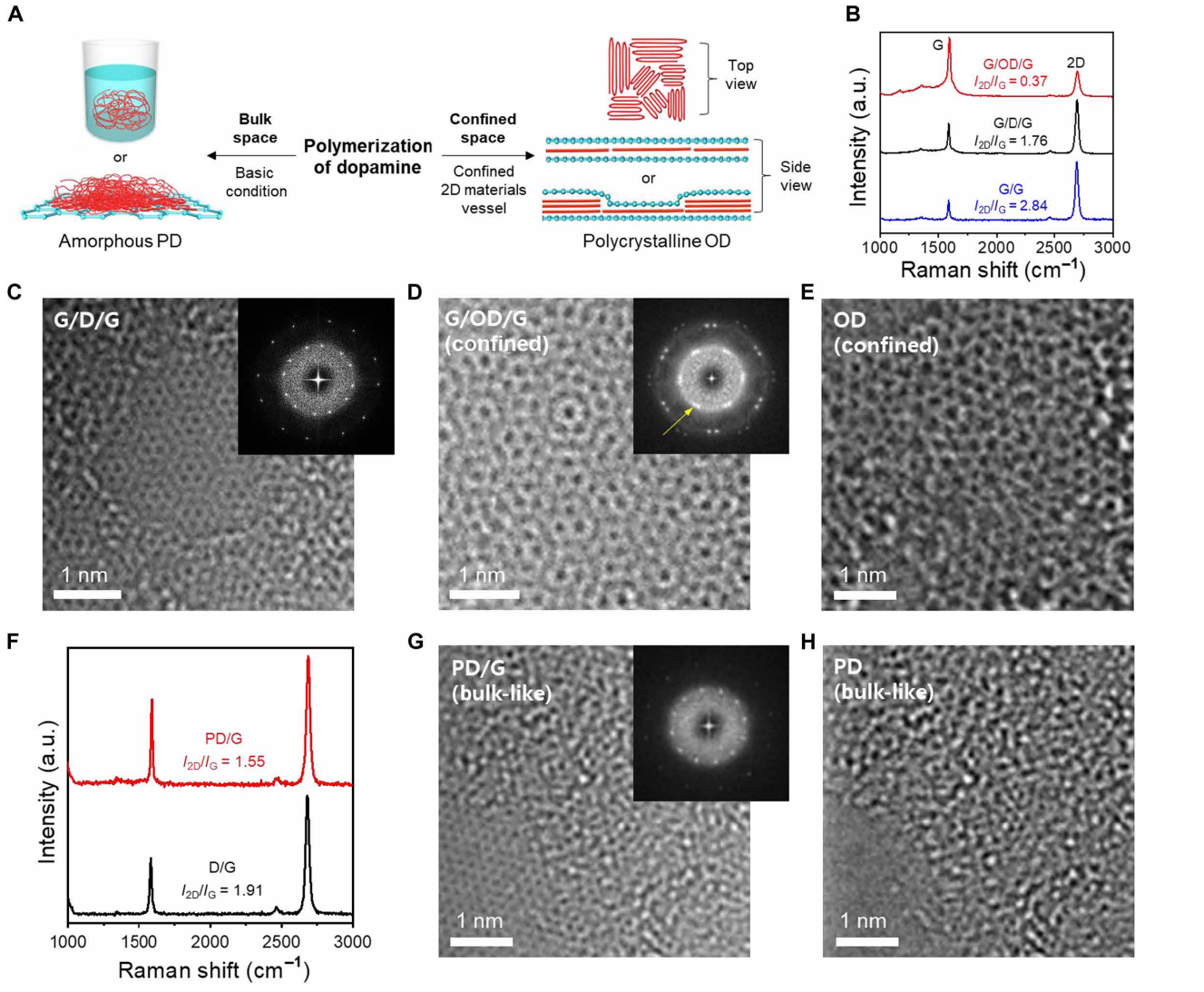

Fig. 3. Polymerization of dopamine in 2D confined space and its characteristics. (**A**) Comparison of formation of amorphous polydopamine (PD) in bulk space and polycrystalline oligodopamine (OD) in confined space. In the top view image, top and bottom graphene layers are omitted. (**B**) Raman spectra of G/G, G/D/G, and G/OD/G. (**C** and **D**) HRTEM image and fast Fourier transform (FFT) (inset of each image) of G/D/G (C) and G/OD/G (confined) (D). After polymerization, the formation of ring patterns in FFT was observed [yellow arrow in inset of (D)]. (**E**) A 2D crystalline sheet was confirmed in IFFT image of (D). Polymerization of dopamine prepared at the bulk scale. (**F**) Comparison of the Raman spectra of D/G and PD/G without a top graphene layer. (**G** and **H**) HRTEM image (G) and IFFT image of PD/G (bulk) (H). Inset of (G) and IFFT image of PD/G revealed that PD is amorphous.

To realize interesting crystalline oligodopamine (OD), the graphene/dopamine/graphene (G/D/G) layers were heated to 180°C for 3 hours. The formation of OD was confirmed by appearance of protonated amine of dopamine (—NH_3^+) and secondary amine of cyclized dopamine (—NH—) at 401.03 and at 398.50 eV, respectively, in the x-ray photoelectron spectroscopy (XPS) profiles (fig. S14B) (*47*–*49*). We also compared the Raman spectra of three samples (G/G, G/D/G, and G/OD/G) (Fig. 3B). The I_{2D}/I_G in G/D/G decreased slightly to 1.76 (black curve in Fig. 3B) from 2.84 in G/G due to π-π interactions between dopamine and graphene (*37*, *38*). A large reduction in I_{2D}/I_G was observed in the G/OD/G sample, which is attributed to the zone-folding effect through superlattice formation (*39*, *40*). This is consistent with the Raman result for G/HBC/G. Moreover, the HRTEM images of G/D/G and G/OD/G showed different moiré patterns (Fig. 3, C and D). The stacking angles of bilayer graphene (top and bottom graphene in the sandwich structures) are different in G/D/G and G/OD/G because the HRTEM images were taken at different positions before and after heating. The fast Fourier transform (FFT) of G/OD/G exhibited ring patterns after polymerization, suggesting that polycrystalline OD has been formed [see the yellow arrow in inset of Fig. 3D and x-ray diffraction (XRD) spectra in fig. S15]. We used the inverse fast Fourier transform (IFFT) technique to remove signals of graphene layers from the HRTEM images. As a result, short-range ordered graphitic domains were observed in G/OD/G (Fig. 3E and fig. S16, A to C). In addition, the cross-sectional TEM images of G/OD/G revealed sheet-like OD layers between top and bottom graphene (figs. S16, D and E, and S17). On the basis of these results, we suggest that the

Downloaded from https://www.science.org on November 25, 2024

OD in the graphene sandwich is a polycrystalline layered structure. The crystallization of OD in the confined 2D space is consistent with recent proposal of partial π-conjugation and π-π stacking of indole moieties in progressive assembly of dopamine for a polydopamine coating (*49*). The structure and exact mechanism of polydopamine have not yet been fully elucidated (*46*, *47*). Thus, we propose that the driving force for polymerization of dopamine in graphene sandwich would be flattening of dopamine by vdW pressure (fig. S18), and more indole skeletons by oxidative ring closure are formed due to the confinement effect by vdW pressure in the graphene sandwich structure (fig. S19). The indole skeletons such as indole-5,6-quinone could be responsible for crystallized form. The molecular weight of the crystallized product is less than 2000 Da because of difficulty in rearrangement or assembly of solid-state dopamine molecules in a large area (fig. S20).

For comparison, we synthesized PD under unconfined conditions on graphene (Fig. 3, F to H). The XPS profile of dopamine on graphene after heating under unconfined conditions revealed polymerization (fig. S14C). However, the formed polydopamine is amorphous in the absence of confining it with top layer graphene. The amorphous polydopamine under unconfined conditions does not exhibit reduction in I_{2D}/I_G ratio (Fig. 3F) or the formation of a ring pattern in the FFT of the TEM image (inset of Fig. 3G). Thus, without confinement, the polydopamine on graphene is similar to bulk amorphous PD (IFFT image; Fig. 3H). We have also compared the reflectance contrast spectra of G/G, PD/G, G/D/G, and G/OD/G (fig. S21A). A negative peak was observed at 520 nm in G/OD/G, indicating enhanced reflectivity due to the polycrystalline structure of OD (*50*, *51*). The simulation result for the reflectance contrast of G/OD/G confirms the presence of a negative peak near 520 nm (fig. S21B).

The crystalline OD between graphene layers forms a composite material with enhanced properties such as lower sheet resistance (344 ohm sq^{-1}) than single-layer (982 ohm sq^{-1}) and two-layer graphene (G/G = 642 ohm sq^{-1}). The enhanced electrical property is attributed to doping of top and bottom graphene layers by nitrogen in the OD. To test the mechanical properties, the bending stability and Young's modulus were determined by measuring the sheet resistance under applied strain (Fig. 4, A and B). The composite G/OD/G maintained its sheet resistance with an applied strain up to 1.3%, while G/G, three-layer graphene, and six-layer graphene demonstrated an increased sheet resistance with an applied strain over 0.6, 0.42, and 0.42%, respectively. The Young's modulus obtained by nanoindentation of G/OD/G (423 GPa) was found to be 41% larger than that of G/G (300 GPa). Furthermore, we also report that the G/OD/G film can serve as a protective layer for water vapor transmission. Figure 4C compares the water vapor transmission rates (WVTRs) of 2DMs on a PET substrate. The WVTR of G/OD/G on PET was found to be 0.08 g m^{-2} day^{-1}, i.e., 99% less than that of PET (1.3 g m^{-2} day^{-1}). The G/OD/G composite exhibits superior performance compared to 2DMs such as single-crystalline hBN, polycrystalline hBN, and graphene layers (*51*–*54*). This is because OD blocks the defects present in the top and bottom graphene layers which can facilitate water vapor transmission.

DISCUSSION

We demonstrated the cyclodehydrogenation of HPB via confinement between graphene layers as a proof of concept. We showed that, although the cyclodehydrogenation of HPB does not proceed at the bulk scale, high pressure in the confined space between two graphene or hBN layers allows the reaction to propagate. Furthermore, we synthesized previously unrealized polycrystalline phase of OD over a large area (5 cm × 5 cm) that shows intriguing electronic, mechanical, and barrier properties. Our results suggest that other functional molecules and materials may be realized through reactions enabled by the high pressure between layers of 2DMs.

MATERIALS AND METHODS

Cyclodehydrogenation of HPB in confined 2DM vessel

First, HPB (98%; Sigma-Aldrich) was dissolved in dichloromethane solution with a concentration of 2 mg ml^{-1}. The HPB was simply spin-coated on the 2DM (graphene and hBN) at 4000 rpm for 60 s. The thickness of spin-coated HPB on graphene was 1.12 nm (see AFM images in fig. S22). A second layer of the 2DM was transferred onto HPB/2DM to fabricate a confined 2DM vessel containing HPB (2DM/HPB/2DM). The transferred G/HPB/G was heated at 65°C to remove the water and enhance the adhesion of graphene. Cyclodehydrogenation of HPB was fully ensured by heating at 200°C, yielding

Downloaded from https://www.science.org on November 25, 2024

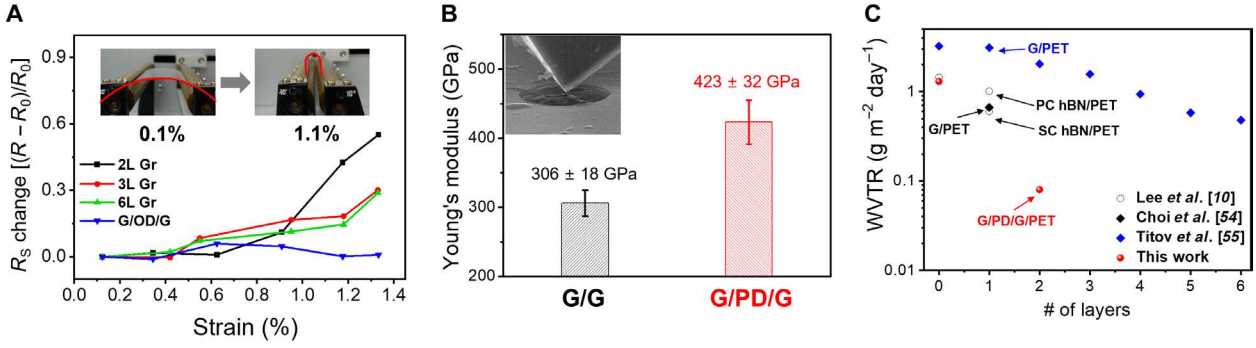

Fig. 4. Physical properties of crystalline OD between graphene layers. (**A**) Bending stability test of few-layer graphene and G/OD/G. G/OD/G maintained their sheet resistances even after applying high strain compared to few-layer graphene. Transmittances of G/G and G/OD/G are 95.4 and 94.84%, respectively. (**B**) Young's modulus of G/G and G/OD/G measured by a nanoindentation test (inset of figure). OD enhanced the Young's modulus of two-layer (2L) graphene by 41%. (**C**) Water vapor transmission rate (WVTR) of G/OD/G and comparison with previous studies. Compared to single-crystal hBN and other results, G/OD/G exhibited excellent WVTR values (0.08 g m^{-2} day^{-1}).

HBC at the end of the reaction. CVD grown graphene was bought from LG Electronics Inc. Trilayer hBN with AA′ stacking order was grown by a remote inductively coupled plasma CVD method. Trilayer hBN was grown on sapphire substrate using borazine (Gelest Inc.) precursor with Ar gas (10 standard cubic centimeter per minute) at 1220°C.

Ni deposition on the 2DM confined vessel

To characterize HPB in the confined 2DM vessel, hBN/HPB/hBN and G/HPB/G were prepared by a simple method. Ni was deposited on 2DM/(HPB or HBC)/2DM by e-beam (20 nm, 2 Å/s) and sputtering (500 nm). After depositing Ni on one side of 2DM/(HPB or HBC)/2DM, the other side was also Ni-deposited to produce Ni/2DM/(HPB or HBC)/2DM/Ni. After Ni deposition on both sides of 2DM/HPB/2DM, the prepared samples were split using a thermal release tape. Since the binding energy between 2DM (graphene and hBN) and Ni is high (*41*), HBC could be extracted from the confined 2DM vessel by this splitting technique.

Preparation of polydopamine by pH control

The polydopamine bulk powder was prepared as follows: First, dopamine solution was prepared by dissolving dopamine HCl in deionized (DI) water. NaOH solution (0.1 M) was used to maintain the pH of the dopamine solution at 8 or higher. After a few days, the dopamine solutions appeared dark brown as a result of self-polymerization, indicating the occurrence of polydopamine. We evaporated the polydopamine solution in a 70°C oven for 1 day to obtain the polydopamine in a powder form.

Monomer preparation in confined 2DM vessel

Dopamine was dissolved in DI water, and pH of the solution was adjusted to 4 to prevent self-polymerization of dopamine. Then, the prepared solution was simply spin-coated on graphene at 4000 rpm for 60 s to give the thickness of about 1.17 nm (see AFM images in fig. S23). A second layer of graphene was transferred onto the solution-coated 2DMs to prepare the 2D confined space containing the target materials. To polymerize monomers in the confined 2DM vessel, the heating method was used (180°C for 3 hours). The prepared oligomers were characterized by Raman spectroscopy, XPS, XRD, and TEM.

Characterization

Raman spectra were measured using a micro Raman spectrometer (alpha 300, WITec GmBH) equipped with a 532-nm laser. To obtain the Raman spectra, the samples were transferred onto SiO_2(300 nm)/Si substrates to amplify the signal by multiple reflection. XPS (K-Alpha, Thermo Fisher Scientific) was performed to determine the chemical compositions of the samples. XRD profiles were recorded by a SmartLab diffractometer (9 kW; Rigaku) with Cu Kα radiation ($\lambda = 1.541$ Å). The XRD system was operated at 45 kV and 200 mA in a two-theta range of 10° to 90° with a theta-to-theta mode. The step size was 0.02°, and the scanning speed was 5°/min. For HRTEM imaging and selected-area electron diffraction measurements, double C_s aberration–corrected TEM (Titan Cube G2 60-300, FEI) was performed at 80 kV using a monochromatic e-beam. After obtaining the HRTEM images, IFFT images were achieved for organic molecules by removing the G/G crystal lattice from FFT to show the clear contrast of organic molecules. The sequential images for the structural change of HPB and HBC molecules were acquired using a Gatan Digital Micrograph script. Each of images was taken with an exposure time of 0.1 s and an interval time of 1.1 s. The reflectance contrast spectrum was obtained using white light excitation (the spectrometer has a spectral range starting from 350 nm). PL spectra were obtained using an excited 340-nm laser. The pulse duration and repetition rate were 180 fs and 80 MHz, respectively. Both reflectance and PL signals were collected by a spectrometer equipped with a thermoelectrically cooled charge-coupled device detector (Andor Inc., DU971P). WVTR was measured by a WVTR analyzer with high sensitivity (Aquatran 2, Mocon). WVTR was measured at 23°C with relative humidity of 100%. The TOF-SIMS measurements were performed with a TOF-SIMS 5 instrument (IONTOF GmbH, Münster, Germany) using 25-keV Bi_3^+ primary ion beam with a current of 0.3 pA in positive ion mode. The TOF-SIMS and Orbitrap-SIMS measurements in fig. S2 (C to F) were performed using a M6 Hybrid SIMS instrument equipped with a 30-keV Bi_3^+ primary ion beam (a current of 0.3 pA) and 10-keV Ar cluster ion beam, respectively, in positive ion mode.

Theoretical calculations

Geometry optimization of G/HPB/G and G/HBC/G was conducted at the B3LYP/6-31G* level of theory with D3 dispersion energy correction based on TeraChem software (*55*). The energy barrier calculations for both synchronous and stepwise mechanisms for an isolated HPB were performed at the same level of theory. Transition state structures were chosen as the maximum energy structures from constrained geometry optimization at variable C─C bond lengths. Pressure (P) was calculated from force components (fig. S12) based solely on hBN bilayers at the optimized hBN/HPB/hBN by $P = \sum_{I \in \mathrm{hBN}} F_{I,\perp}/A$, where $F_{I,\perp}$ is the force component normal to the central benzene ring of HPB for the Ith atom in the hBN layers. The area of a molecule was chosen as ~154 Å^2 approximated from a circle with a diameter of ~14 Å (distance from farthest hydrogen atoms).

Supplementary Materials

The PDF file includes:

Figs. S1 to S23
Legends for movies S1 and S2
Legend for data S1
References

Other Supplementary Material for this manuscript includes the following:

Movies S1 and S2
Data S1

REFERENCES AND NOTES

1. E. Snider, N. Dasenbrock-Gammon, R. McBride, M. Debessai, H. Vindana, K. Vencatasamy, K. V. Lawler, A. Salamat, R. P. Dias, Room-temperature superconductivity in a carbonaceous sulfur hydride. *Nature.* **586**, 373–377 (2020).
2. F. Ke, L. Zhang, Y. Chen, K. Yin, C. Wang, Y.-K. Tzeng, Y. Lin, H. Dong, Z. Liu, J. S. Tse, W. L. Mao, J. Wu, B. Chen, Synthesis of atomically thin hexagonal diamond with compression. *Nano Lett.* **20**, 5916–5921 (2020).
3. G. Algara-Siller, O. Lehtinen, F. C. Wang, R. R. Nair, U. Kaiser, H. A. Wu, A. K. Geim, I. V. Grigorieva, Square ice in graphene nanocapillaries. *Nature.* **519**, 443–445 (2015).
4. L. Wang, L. Liu, J. Chen, A. Mohsin, J. H. Yum, T. W. Hudnall, C. W. Bielawski, T. Rajh, X. Bai, S.-P. Gao, G. Gu, Synthesis of honeycomb-structured beryllium oxide via graphene liquid cells. *Angew. Chem. Int. Ed.* **59**, 15734–15740 (2020).
5. T. Lehnert, M. K. Kinyanjui, A. Ladenburger, D. Rommel, K. Wörle, F. Börrnert, K. Leopold, U. Kaiser, In Situ crystallization of the insoluble anhydrite all phase in graphene pockets. *ACS Nano.* **11**, 7967–7973 (2017).
6. K. S. Vasu, E. Prestat, J. Abraham, J. Dix, R. J. Kashtiban, J. Beheshtian, J. Sloan, P. Carbone, M. Neek-Amal, S. J. Haigh, A. K. Geim, R. R. Nair, Van der Waals pressure and its effect on trapped interlayer molecules. *Nat. Commun.* **7**, 12168 (2016).

Downloaded from https://www.science.org on November 25, 2024

7. C. H. Y. X. Lim, M. Nesladek, K. P. Loh, Observing high-pressure chemistry in graphene bubbles. *Angew. Chem. Int. Ed.* **53**, 215–219 (2014).
8. J. M. Yuk, J. Park, P. Ercius, K. Kim, D. J. Hellebusch, M. F. Crommie, J. Y. Lee, A. Zettl, A. P. Alivisatos, High-resolution EM of colloidal nanocrystal growth using graphene liquid cells. *Science.* **336**, 61–64 (2012).
9. J. Park, H. Elmlund, P. Ercius, J. M. Yuk, D. T. Limmer, Q. Chen, K. Kim, S. H. Han, D. A. Weitz, A. Zettl, A. P. Alivisatos, 3D structure of individual nanocrystals in solution by electron microscopy. *Science.* **349**, 290–295 (2015).
10. Z. Lee, K.-J. Jeon, A. Dato, R. Erni, T. J. Richardson, M. Frenklach, V. Radmilovic, Direct imaging of soft–hard interfaces enabled by graphene. *Nano Lett.* **9**, 3365–3369 (2009).
11. A. Kolmakov, D. A. Dikin, L. J. Cote, J. Huang, M. K. Abyaneh, M. Amati, L. Gregoratti, S. Günther, M. Kiskinova, Graphene oxide windows for in situ environmental cell photoelectron spectroscopy. *Nat. Nanotechnol.* **6**, 651–657 (2011).
12. A. B. Grommet, M. Feller, R. Klajn, Chemical reactivity under nanoconfinement. *Nat. Nanotechnol.* **15**, 256–271 (2020).
13. F. J. Rizzuto, L. K. S. V. Krbek, J. R. Nitschke, Strategies for binding multiple guests in metal–organic cages. *Nat. Rev. Chem.* **3**, 204–222 (2019).
14. H. G. Hansma, Possible origin of life between mica sheets. *J. Theor. Biology.* **266**, 175–188 (2010).
15. Q. Zhang, K. Tiefenbacher, Terpene cyclization catalysed inside a self-assembled cavity. *Nat. Chem.* **7**, 197–202 (2015).
16. H. Xu, J. Gao, D. Jiang, Stable, crystalline, porous, covalent organic frameworks as a platform for chiral organocatalysts. *Nat. Chem.* **7**, 905–912 (2015).
17. S. H. Ko, T. Lee, H. Park, D.-S. Ahn, K. Kim, Y. Kwon, S. J. Cho, R. Ryoo, Nanocage-confined synthesis of fluorescent polycyclic aromatic hydrocarbons in zeolite. *J. Am. Chem. Soc.* **140**, 7101–7107 (2018).
18. D. J. Hornbaker, S.-J. Kahng, S. Misra, B. W. Smith, A. T. Johnson, E. J. Mele, D. E. Luzzi, A. Yazdani, Mapping the one-dimensional electronic states of nanotube peapod structures. *Science.* **295**, 828–831 (2002).
19. M. Koshino, Y. Niimi, E. Nakamura, H. Kataura, T. Okazaki, K. Suenaga, S. Iijima, Analysis of the reactivity and selectivity of fullerene dimerization reactions at the atomic level. *Nat. Chem.* **2**, 117–124 (2010).
20. H. Takezawa, M. Fujita, Molecular confinement effects by self-assembled coordination cages. *Bull. Chem. Soc. Jpn.* **94**, 2351–2369 (2021).
21. E. G. Percastegui, T. K. Ronson, J. R. Nitschke, Design and applications of water-soluble coordination cages. *Chem. Rev.* **120**, 13480–13544 (2020).
22. H. Li, J. Xiao, Q. Fu, X. Bao, Confined catalysis under two-dimensional materials. *Proc. Natl. Acad. Sci. U.S.A.* **114**, 5930–5934 (2017).
23. D. Deng, K. S. Novoselov, Q. Fu, N. Zheng, Z. Tian, X. Bao, Catalysis with two-dimensional materials and their heterostructures. *Nat. Nanotechnol.* **11**, 218–230 (2016).
24. M. Kolmer, A.-K. Steiner, I. Izydorczyk, W. Ko, M. Engelund, M. Szymonski, A.-P. Li, K. Amsharov, Rational synthesis of atomically precise graphene nanoribbons directly on metal oxide surfaces. *Science.* **369**, 571–575 (2020).
25. J. Cai, P. Ruffieux, R. Jaafar, M. Bieri, T. Braun, S. Blankenburg, M. Muoth, A. P. Seitsonen, M. Saleh, X. Feng, K. Müllen, R. Fasel, Atomically precise bottom-up fabrication of graphene nanoribbons. *Nature.* **466**, 470–473 (2010).
26. J. Cai, C. A. Pignedoli, L. Talirz, P. Ruffieux, H. Söde, L. Liang, V. Meunier, R. Berger, R. Li, X. Feng, K. Müllen, R. Fasel, Graphene nanoribbon heterojunctions. *Nat. Nanotechnol.* **9**, 896–900 (2014).
27. Y.-C. Chen, T. Cao, C. Chen, Z. Pedramrazi, D. Haberer, D. G. de Oteyza, F. R. Fischer, S. G. Louie, M. F. Crommie, Molecular bandgap engineering of bottom-up synthesized graphene nanoribbon heterojunctions. *Nat. Nanotechnol.* **10**, 156–160 (2015).
28. M. Stępień, E. Gońka, M. Żyła, N. Sprutta, Heterocyclic nanographenes and other polycyclic heteroaromatic compounds: Synthetic routes, properties, and applications. *Chem. Rev.* **117**, 3479–3716 (2017).
29. P. Rempala, J. Kroulík, B. T. King, A slippery slope: Mechanistic analysis of the intramolecular scholl reaction of hexaphenylbenzene. *J. Am. Chem. Soc.* **126**, 15002–15003 (2004).
30. V. L. Nguyen, D. J. Perello, S. Lee, C. T. Nai, B. G. Shin, J.-G. Kim, H. Y. Park, H. Y. Jeong, J. Zhao, Q. A. Vu, S. H. Lee, K. P. Loh, S.-Y. Jeong, Y. H. Lee, Wafer-scale single-crystalline AB-stacked bilayer graphene. *Adv. Mater.* **28**, 8177–8183 (2016).
31. C.-J. Kim, A. Sánchez-Castillo, Z. Ziegler, Y. Ogawa, C. Noguez, J. Park, Chiral atomically thin films. *Nat. Nanotechnol.* **11**, 520–524 (2016).
32. L. Dong, P. N. Liu, N. Lin, Surface-activated coupling reactions confined on a surface. *Acc. Chem. Res.* **48**, 2765–2774 (2015).
33. J. Yang, N. Song, Q. Jia, Investigation of the surface confinement effect of copper nanoclusters: Construction of an ultrasensitive fluorescence turn-on bio-enzyme sensing platform. *Nanoscale.* **11**, 21927–21933 (2019).
34. P. Chandra, A. M. Jonas, A. E. Fernandes, Sequence and surface confinement direct cooperativity in catalytic precision oligomers. *J. Am. Chem. Soc.* **140**, 5179–5184 (2018).
35. A. C. Ferrari, D. M. Basko, Raman spectroscopy as a versatile tool for studying the properties of graphene. *Nat. Nanotechnol.* **8**, 235–246 (2013).
36. L. M. Malard, M. A. Pimenta, G. Dresselhaus, M. S. Dresselhaus, Raman spectroscopy in graphene. *Phys. Rep.* **473**, 51–87 (2009).
37. A. Das, S. Pisana, B. Chakraborty, S. Piscanec, S. K. Saha, U. V. Waghmare, K. S. Novoselov, H. R. Krishnamurthy, A. K. Geim, A. C. Ferrari, A. K. Sood, Monitoring dopants by Raman scattering in an electrochemically top-gated graphene transistor. *Nat. Nanotechnol.* **3**, 210–215 (2008).
38. X. Dong, D. Fu, W. Fang, Y. Shi, P. Chen, L.-J. Li, Doping single-layer graphene with aromatic molecules. *Small.* **5**, 1422–1426 (2009).
39. N. Jung, B. Kim, A. C. Crowther, N. Kim, C. Nuckolls, L. Brus, Optical reflectivity and raman scattering in few-layer-thick graphene highly doped by K and Rb. *ACS Nano* **5**, 5708–5716 (2011).
40. V. Carozo, C. M. Almeida, B. Fragneaud, P. M. Bedê, M. V. O. Moutinho, J. Ribeiro-Soares, N. F. Andrade, A. G. Souza Filho, M. J. S. Matos, B. Wang, M. Terrones, R. B. Capaz, A. Jorio, C. A. Achete, L. G. Cançado, Resonance effects on the Raman spectra of graphene superlattices. *Phys. Rev. B.* **88**, 085401 (2013).
41. J. Kim, H. Park, J. B. Hannon, S. W. Bedell, K. Fogel, D. K. Sadana, C. Dimitrakopoulos, Layer-resolved graphene transfer via engineered strain layers. *Science.* **342**, 833–836 (2013).
42. C.-Y. Tsai, Q. Zhang, Y.-Z. Wang, J. Shyong, H. L. Chen, D.-J. Liaw, Enhancing the emission of hexa-peri-hexabenzocoronene-containing polynorbornene via electron donating, unsymmetric constitution and solvent effects. *Polym. Chem.* **8**, 3327–3332 (2017).
43. T. T. Tran, K. Bray, M. J. Ford, M. Toth, I. Aharonovich, Quantum emission from hexagonal boron nitride monolayers. *Nat. Nanotechnol.* **11**, 37–41 (2016).
44. T. T. Tran, K. Bray, M. J. Ford, M. Toth, I. Aharonovich, Nanobubbles at GPa pressure under graphene. *Nano Lett.* **15**, 6162–6169 (2015).
45. X. Du, L. Li, J. Li, C. Yang, N. Frenkel, A. Welle, S. Heissler, A. Nefedov, M. Grunze, P. A. Levkin, UV-triggered dopamine polymerization: Control of polymerization, surface coating, and photopatterning. *Adv. Mater.* **26**, 8029–8033 (2014).
46. H. Lee, S. M. Dellatore, W. M. Miller, P. B. Messersmith, Mussel-inspired surface chemistry for multifunctional coatings. *Science.* **318**, 426–430 (2007).
47. J. Liebscher, R. Mrówczyński, H. A. Scheidt, C. Filip, N. D. Hădade, R. Turcu, A. Bende, S. Beck, Structure of polydopamine: A never-ending story? *Langmuir.* **29**, 10539–10548 (2013).
48. W. Xu, Z. Qin, C.-T. Chen, H. R. Kwag, Q. Ma, A. Sarkar, M. J. Buehler, D. H. Gracias, Ultrathin thermoresponsive self-folding 3D graphene. *Sci. Adv.* **3**, e1701084 (2017).
49. S. Hong, Y. Wang, S. Y. Park, H. Lee, Progressive fuzzy cation-π assembly of biological catecholamines. *Sci. Adv.* **4**, eaat7457 (2018).
50. M. Bouška, S. Pechev, Q. Simon, R. Boidin, V. Nazabal, J. Gutwirth, E. Baudet, P. Němec, Pulsed laser deposited GeTe-rich GeTe-Sb2Te3 thin films. *Sci. Rep.* **6**, 26552 (2016).
51. C. Koch, G. Schienke, M. Paulsen, D. Meyer, M. Wimmer, H. Volker, M. Wuttig, W. Bensch, Investigating the influence of resonant bonding on the optical properties of phase change materials (GeTe)xSnSb2Se4. *Chem. Mater.* **29**, 9320–9327 (2017).
52. J. S. Lee, S. H. Choi, S. J. Yun, Y. I. Kim, S. Boandoh, J.-H. Park, B. G. Shin, H. Ko, S. H. Lee, Y.-M. Kim, Y. H. Lee, K. K. Kim, S. M. Kim, Wafer-scale single-crystal hexagonal boron nitride film via self-collimated grain formation. *Science.* **362**, 817–821 (2018).
53. T. H. Seo, S. Lee, H. Cho, S. Chandramohan, E. K. Suh, H. S. Lee, S. K. Bae, S. M. Kim, M. Park, J. K. Lee, M. J. Kim, Tailored CVD graphene coating as a transparent and flexible gas barrier. *Sci. Rep.* **6**, 24143 (2016).
54. K. Choi, S. Nam, Y. Lee, M. Lee, J. Jang, S. J. Kim, Y. J. Jeong, H. Kim, S. Bae, J.-B. Yoo, S. M. Cho, J.-B. Choi, H. K. Chung, J.-H. Ahn, C. E. Park, B. H. Hong, Reduced water vapor transmission rate of graphene gas barrier films for flexible organic field-effect transistors. *ACS Nano.* **9**, 5818–5824 (2015).
55. A. V. Titov, I. S. Ufimtsev, N. Luehr, T. J. Martinez, Generating efficient quantum chemistry codes for novel architectures. *J. Chem. Theory Comput.* **9**, 213–221 (2013).
56. J. C. Vickerman, A. Brown, N. M. Reed, Eds. in *Secondary Ion Mass Spectrometry, Principles and Applications* (Oxford University Press, 1989).
57. M. K. Passarelli, A. Pirkl, R. Moellers, D. Grinfeld, F. Kollmer, R. Havelund, C. F. Newman, P. S. Marshall, H. Arlinghaus, M. R. Alexander, A. West, S. Horning, E. Niehuis, A. Makarov, C. T. Dollery, I. S. Gilmore, The 3D OrbiSIMS—Label-free metabolic imaging with subcellular lateral resolution and high mass-resolving power. *Nat. Methods* **14**, 1175–1183 (2017).
58. M. P. Seah, R. Havelund, I. S. Gilmore, Universal equation for argon cluster size-dependence of secondary ion spectra in SIMS of organic materials. *Phys. Chem. C.* **118**, 12862–12872 (2014).
59. L. Novotny, B. Hecht, *Principles of Nano-optics* (Cambridge University Press, 2012).

Acknowledgments: We thank J. S. Jin for measurement and discussion of TOF-SIMS and OribSIMS spectra by hybrid SIMS. **Funding:** This work was supported by the research fund (NRF-2019R1A4A1027934 to Y.S.P. and NRF-2020M3D1A1110548 and NRF-2021R1A3B1077184 to H.S.S.) via the National Research Foundation and the Institute for Basic Science (IBS-R019-D1 to S.K.M., IBS-R019-G1 to Z.L., and IBS-R036-D1 to H.S.S.) by the Ministry of Science and ICT, South Korea. **Author contributions:** H.S.S., Z.L., S.K.M., and Y.S.P. planned and supervised this

Downloaded from https://www.science.org on November 25, 2024

project. S.I.Y., Y.L., and K.Y.M. performed cyclodehydrogenation and polymerization in confined 2DM vessels. A.G. performed STM experiments on cyclodehydrogenation of HPB on Au substrate for comparison. H.P., S.S., J.L., M.C., and Z.L. analyzed and simulated TEM data. K.K., C.G., J.S.L., and Y.S.P. synthesized and characterized HPB and HBC. C.G. and Y.J.K. synthesized and characterized XRD spectrum of G/D/G and G/OD/G. D.H., S.W.M., and S.K.M. performed theoretical calculations related to HPB and HPC. Y.D. and F.D. performed calculations on optimized structure of dopamine in graphene sandwich. S.-Y.P. and J.-Y.K. performed the nanoindentation test. Y.-J.K. and W.S.Y. measured the bending stability of G/G and G/PD/G. Y.-J.K. and S.A. performed the WVTR test. S.K. and S.R. measured absorption and PL spectra of G/HPB/G and G/HBC/G. A.G. and A.T. performed the measurement and simulation for reflection contrast of G/PD/G samples. J.S. and J.-Y.K. advised the Ni deposition method to split 2D confined vessels. All authors contributed to the writing of the manuscript and agreed on its contents. **Competing interests:** A patent including crystallization and polymerization in confined 2DM vessels in this work (Korea patent application number is 10-2020-0056497) has been filed by UNIST, Republic of Korea. The authors declare that they have no other competing interests. **Data and materials availability:** All data needed to evaluate the conclusions in the paper are present in the paper and/or the Supplementary Materials.

Submitted 23 April 2024
Accepted 4 October 2024
Published 8 November 2024
10.1126/sciadv.adp9804

Downloaded from https://www.science.org on November 25, 2024